ELSEVIER

Marine and Petroleum Geology 18 (2001) 779–797

Marine and Petroleum Geology

www.elsevier.com/locate/marpetgeo

Salt diapirs in the Dead Sea basin and their relationship to Quaternary extensional tectonics

Abdallah Al-Zoubi[a,1], Uri S. ten Brink[b,*]

[a]*Woods Hole Oceanographic Institution, Woods Hole, MA 02543, USA*
[b]*US Geological survey, Woods Hole Field Center, 384 Woods Hole Road, Woods Hole, MA 02543, USA*

Received 21 March 2001; received in revised form 23 May 2001; accepted 23 May 2001

Abstract

Regional extension of a brittle overburden and underlying salt causes differential loading that is thought to initiate the rise of reactive diapirs below and through regions of thin overburden. We present a modern example of a large salt diapir in the Dead Sea pull-apart basin, the Lisan diapir, which we believe was formed during the Quaternary due to basin transtension and subsidence. Using newly released seismic data that are correlated to several deep wells, we determine the size of the diapir to be 13 × 10 km, its maximum depth 7.2 km, and its roof 125 m below the surface. From seismic stratigraphy, we infer that the diapir started rising during the early to middle Pleistocene as this section of the basin underwent rapid subsidence and significant extension of the overburden. During the middle to late Pleistocene, the diapir pierced through the extensionally thinned overburden, as indicated by rim synclines, which attest to rapid salt withdrawal from the surrounding regions. Slight positive topography above the diapir and shallow folded horizons indicate that it is still rising intermittently. The smaller Sedom diapir, exposed along the western bounding fault of the basin is presently rising and forms a 200 m-high ridge. Its initiation is explained by localized E–W extension due monoclinal draping over the edge of a rapidly subsiding basin during the early to middle Pleistocene, and its continued rise by lateral squeezing due to continued rotation of the Amazyahu diagonal fault. © 2001 Elsevier Science Ltd. All rights reserved.

Keywords: Salt tectonics; Dead Sea basin; Middle East; Dead Sea transform Fault

1. Introduction

Salt tectonics has captured the imagination of geologists for over 150 years (e.g. Jackson, 1995), because a wide variety of salt structures can be generated by the unusual rheology of the salt. Unlike most sedimentary rocks, salt has low effective viscosity, because the minute traces of water in it allow it to deform in solution-transfer creep in low temperatures, low strain rates, and low deviatoric stress (e.g. Wawersik & Zeuch, 1986). The view of viscous deformation was traditionally expanded to include not only the salt but also the sedimentary overburden (see review by Jackson, 1995). In particular, salt diapirism was viewed to result from gravitational (Rayleigh–Taylor) instability due to a dense fluid overburden overlying a less dense fluid salt (Nettleton, 1934). The thicker the overburden, the more unstable the salt was thought to become, and the more likely it was to rise. This approach has been called into question during the last decade because the sedimentary overburden typically shows brittle deformation (e.g. Vendeville & Jackson, 1992a). Analog modeling has shown that diapirs can develop, regardless of density ratio, under thin overburden when the overburden has differential thickness (Vendeville & Jackson, 1992a,b). Differential overburden loading can develop by uneven sedimentation, erosion, or deformation. An example of the latter in extensionally formed grabens is presented here.

Salt tectonics is widespread in many continental margins such as in the Gulf of Mexico and the North Sea (Jackson, Roberts, & Snelson, 1995). The study of diapiric mechanisms in these environments is often hampered, however, by the fact that the salt layer was deposited tens of millions of years ago and has often had a long deformation history. In addition, the source for the salt is sometimes buried deep below the surface and even the roof of the diapirs may be deeply buried. The Dead Sea basin, in contrast, offers a good opportunity to study the development of a modern salt diapir within a fairly simple and well-constrained tectonic deformation regime. The Dead Sea basin is a large pull-apart

* Corresponding author. Tel.: +1-508-457-2396; fax: +1-508-457-2310.
E-mail address: utenbrink@usgs.gov (U.S. ten Brink).

[1] On leave from the Natural Resources Authority, P.O. Box 7, Amman, Jordan.

0264-8172/01/$ - see front matter © 2001 Elsevier Science Ltd. All rights reserved.
PII: S0264-8172(01)00031-9

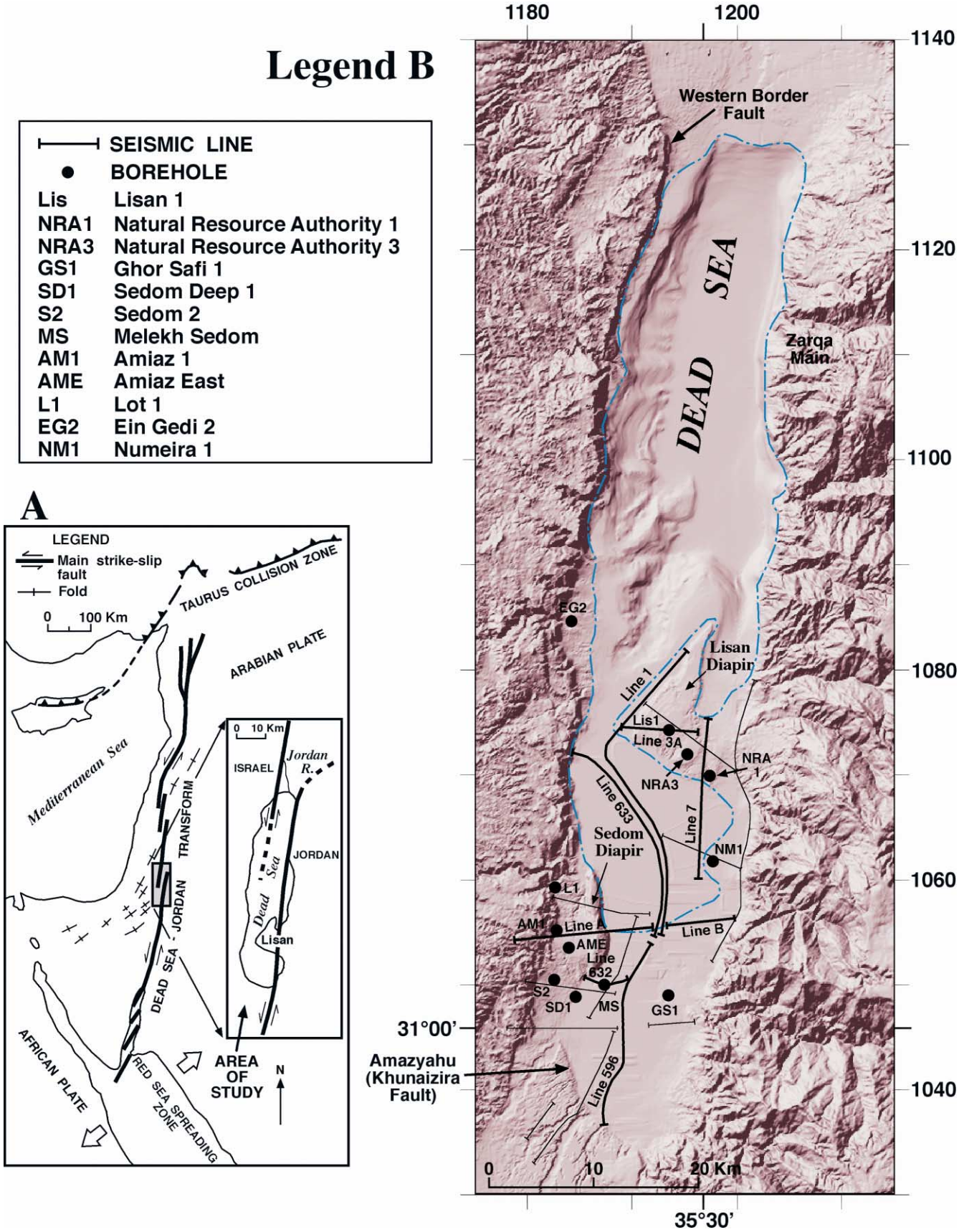

Fig. 1. (A) Outline of the Dead Sea transform and the main strike-slip faults (Modified from Gardosh et al., 1997). (B) Location map of the seismic lines shown in the paper, the boreholes used for interpretation, and Lisan and Sedom diapirs, superimposed on shaded-relief image of the Dead Sea basin (Hall, 1993). Blue dashed dotted line — 1967 coastline of the Dead Sea (after Neev & Hall, 1979). Coordinates in Cassini Palestine grid.

basin within the Dead Sea transform, whose fill includes a salt layer surrounded by fluvial and lacustrine sediments. Diapiric rise may have started not too long after the deposition of the salt layer and is continuing to the present in at least two well-defined diapirs, the Lisan and Sedom diapirs.

The purpose of this study is to understand diapiric growth in the context of basin evolution. Are the diapirs controlled by the transtensional history of the Dead Sea basin, or are they an independent sedimentary phenomenon? To answer this question, we use newly released seismic reflection data from Jordan as well as previously published profiles from Israel. Well data are used to calibrate the seismic data, and potential field data are used to support the interpretation. In addition to addressing the salt tectonics problem, these data are also used to improve on our knowledge of the structure of the basin.

2. Background

2.1. Evaporites in the Dead Sea

The Dead Sea basin is located within the Dead Sea rift, a sinistral transform plate boundary separating the African plate on the west and Arabian plate on the east (Fig. 1). It is the largest basin in the transform valley (e.g. ten Brink et al., 1999). The basin is 135 km long, and 20 km wide. It was interpreted from gravity data to be up to 10 km deep (ten Brink, Ben-Avraham, Bell, Hassouneh, Coleman, Andreasen et al., 1993), but there was previously no seismic evidence to confirm the depth of the basin. The northern 50 km-long part of the basin, the Dead Sea, is a hypersaline lake with a minimum elevation of 720 m below sea level (b.s.l), whereas the southern part of the basin is subaerial with a minimum elevation of 410 m b.s.l. Basin fill consists of lacustrine and fluvial sediments that were deposited in the basin since the middle to late Miocene (Fig. 2). These continental sediments lack suitable fauna for dating. A mostly evaporitic sequence, the Sedom Formation is also present within the basin fill. The formation, as defined in the Sedom diapir, consists of about 80% halite, with the remainder gypsum, marly chalk, dolomite and shale (Zak, 1967). Strontium isotope ratios indicate that the chemical composition of the evaporites is the result of mixing

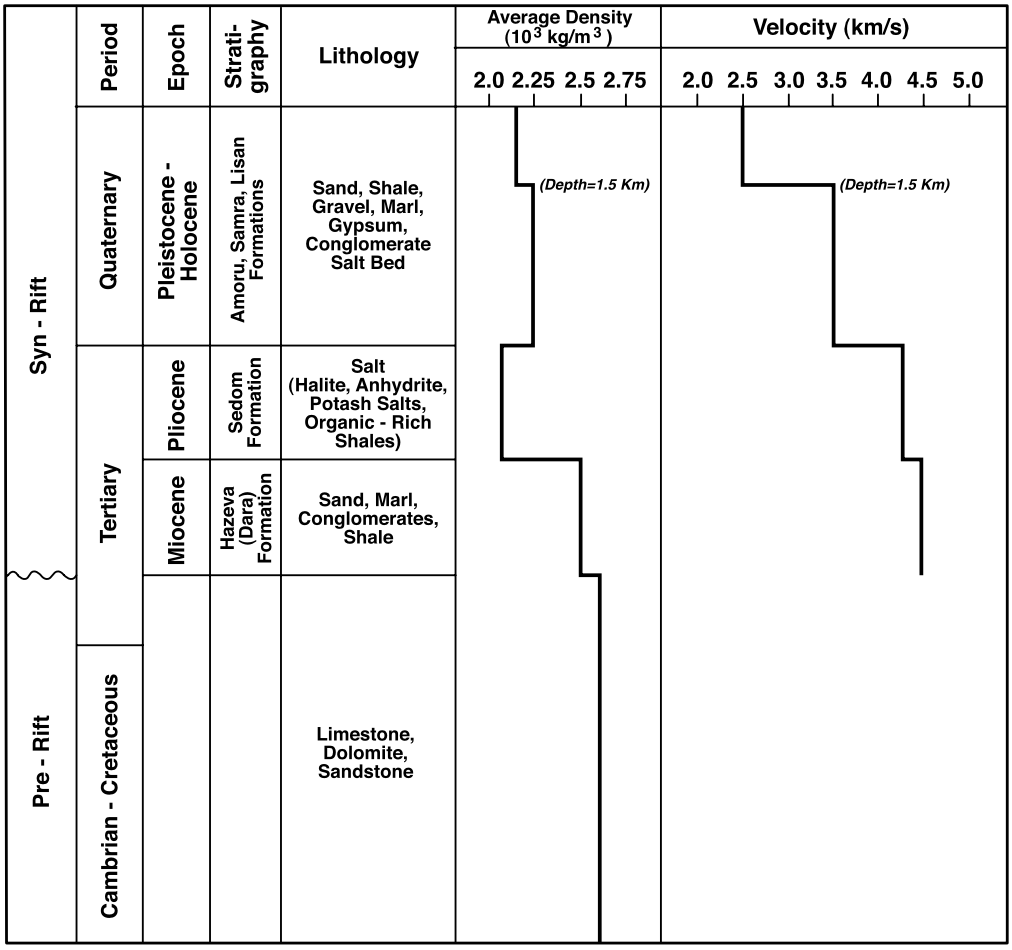

Fig. 2. Generalized stratigraphy of the Dead Sea basin (Al-Khalidi et al., 1997; Kashai & Crocker, 1987), and simplified velocity (Rybakov, pers. commun., 2000) and density (Rybakov et al., 1999 and Qabbani, pers. commun., 2000) curves for the basin fill and the pre-rift sediments. See Gardosh et al. (1997), for detailed stratigraphic logs of the boreholes. The velocity curve, which is based on Sedom Deep borehole sonic log, was used to convert two way travel time of horizons in the seismic reflection profiles to depth. The density curve, which is based on Sedom Deep 1 and Numeira boreholes, was used for gravity modeling.

between seawater, fresh water, and the limestone rock wall of the basin (Stein et al., 2000). The age of the Sedom Formation is estimated to be Pliocene from palynological evidence (Horowitz, 1987) although the lower part may be older (Garfunkel, 1997). Zak (1967) noted that evaporite deposition is potentially very rapid, five or more times faster than deposition of clastics, provided there is an adequate brine supply. The time span for the deposition of the 2 km-thick evaporite bed could have been as short as 0.2 m.y. (Garfunkel, 1997), but data to constrain the time span of deposition are not available.

The Lisan Peninsula, previously a peninsula within the lake, but now at the southern edge of the shrinking lake, is a structurally complex region elevated by the large Lisan salt diapir. Surface elevation of the peninsula is nowhere higher than 50 m above the adjacent basin to the south. The salt diapir is covered by 125 m or more of upper Pleistocene (Lisan Formation) and Holocene sediments. More than 3.5 km of halite was drilled in the Lisan Diapir at the Lisan-1 borehole (Fig. 1; Bender, 1974). Another salt diapir, the Sedom diapir (Fig. 1), is located to the southwest. The diapir has pierced the surface creating a ~200 m high ridge (Zak, 1967) where an approximately 2 km thick section is exposed. The diapir has been rising throughout the Holocene, locally at a rate of 6–7 mma^{-1} (Frumkin, 1996). Additional salt diapirs were inferred by Neev and Hall (1979) from the distribution of shallow halokinetic structure in seismic reflection data in the lake along the western longitudinal fault (see Fig. 3 for location), but a salt layer was not encountered in Ein Gedi-2 borehole, which penetrated into the pre-basin sequence. Salt was also encountered at Sedom-Deep 1 and Amiaz East boreholes as a layer within the basin sedimentary fill (Gardosh, Kashai, Salhov, Shulman, & Tannenbaum, 1997), and is inferred from seismic reflection profiles to underlie the basin southward at least to the Amazyahu Fault (ten Brink & Ben-Avraham, 1989; Gardosh et al., 1997; Kashai & Crocker, 1987). Garfunkel (1997) estimated that the original thickness of the evaporite layer was approximately 2 km, indicating that the basin subsided by, at least, that amount during or before the time of deposition.

The evaporites in the Dead Sea basin were deposited via an ingression of the Mediterranean Sea through northern Israel to the Dead Sea rift about 80 km north of the Dead Sea (Zak, 1967). Connection to the Mediterranean Sea was permanently severed during the Pleistocene when the land west of the rift valley began to rise. There was never a connection to the Dead Sea from the Gulf of Aqaba to the south, where the intervening rift valley is up to 200 m above sea level.

2.2. Structure of the basin

The Dead Sea basin is a pull-apart basin formed between sinistral, left-stepping en-echelon strike-slip faults (Fig. 3). The step may have migrated northward with time (ten Brink & Ben-Avraham, 1989), because of depocenter shift northward of with time (ten Brink et al., 1999; Zak & Freund, 1981). It was proposed on the basis of subsurface seismic data that several diagonal faults, such as the Amazyahu (Khunaizira), Boqeq, and Ein Gedi Faults (Fig. 3) cross the basins at intervals of 20–30 km (Ben-Avraham, ten Brink & Charrach, 1990; Neev & Hall, 1979). The center of the Dead Sea basin has a full graben geometry (Al-Zoubi, Shulman & Ben-Avraham, 2001; Neev & Hall, 1979) indicating that both the eastern and the western bounding faults are overlapping and are both active. The eastern bounding fault, the Wadi Araba Fault (Fig. 3), runs parallel to the eastern shore of the Dead Sea as a single major basin boundary fault. We propose here that a narrow block of intermediate depth ('median block') exists along part of the eastern boundary of the basin. The median block is separated from the deep part of the basin by the Ghor Safi Fault.

Strike slip in the western side of the basin is accommodated along a fault separating the deep part of the basin from the western median block, (ten Brink & Ben-Avraham, 1989; Neev & Hall, 1979) henceforth, referred to as the western longitudinal Fault or as the Sedom Fault near the Sedom diapir. The escarpment bounding the basin west of the western median block is a normal fault, which accommodates tensile stresses caused by the creation of a topographic step (ten Brink & Ben-Avraham, 1989) as evidenced from the vertical slicken lines, (Frieslander & Ben-Avraham, 1989).

3. Interpretation

3.1. Seismic reflection data

The interpreted geophysical data consist of newly released as well as published seismic reflection data (Al-Zoubi et al., 2000; Ben-Avraham et al., 1990; ten Brink & Ben-Avraham, 1989; Csato, Kendall, Nairm, & Baum, 1997; Gardosh et al., 1997; Kashai & Crocker, 1987) and of gravity and new magnetic data. A dense grid of seismic reflection profiles has been collected during the last three decades in support of oil exploration. There were often difficulties in acquiring good quality seismic data, especially at greater depths, because of poor coupling due to unconsolidated gravel at shallow depths. In addition, the narrow geometry of the Dead Sea rift and the various man-made and industrial obstacles (Arab Potash Company and Dead Sea Works) govern the direction and the length of the lines. The geometry is in effect even narrower because surveys could not cross the international border along the middle of the valley. The average length of the cross lines from each side (Jordan and Israel) is about 6–8 km.

Our interpretation of the seismic data is based on the lithostratigaphic data obtained from boreholes in the area (Sedom Deep 1; Amiaz East; Melekh Sedom 1, Lisan 1;

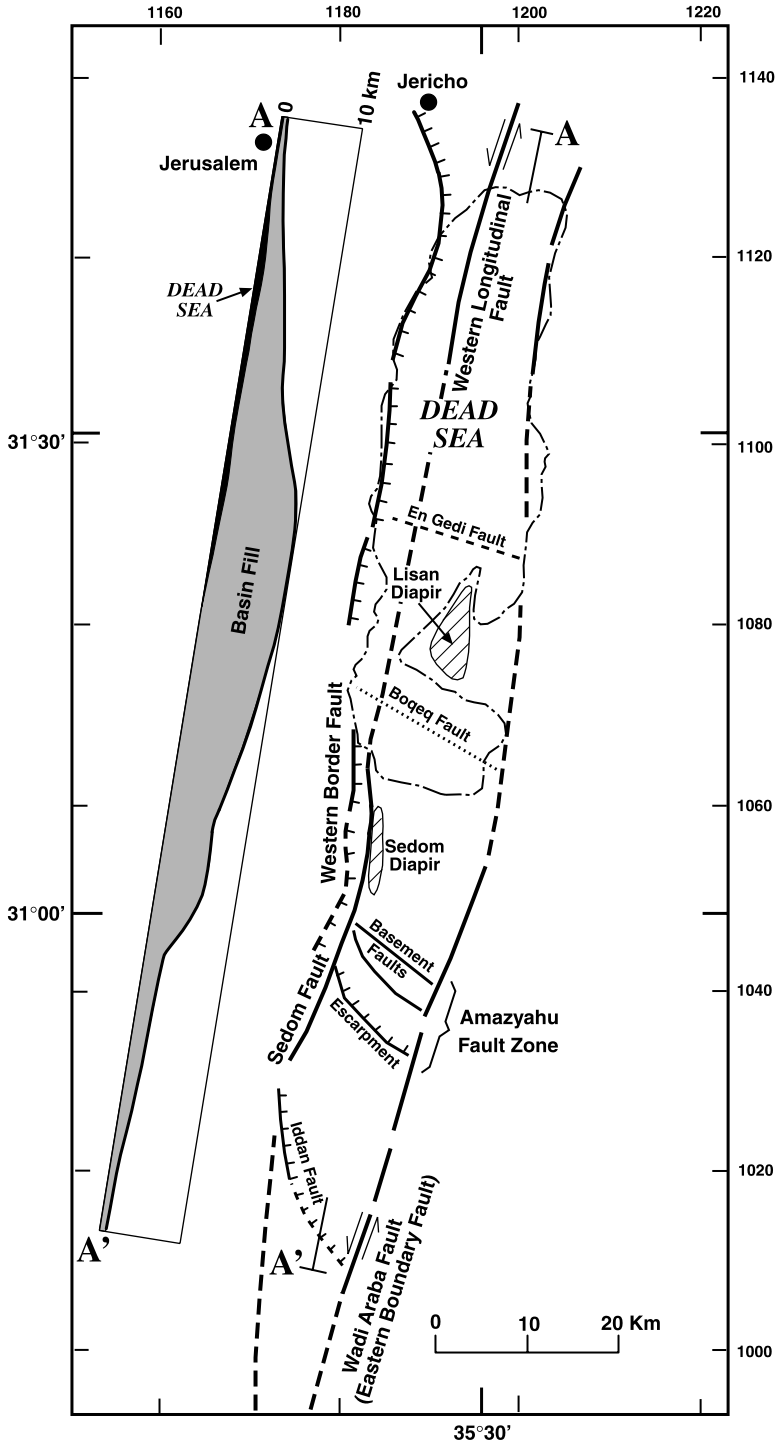

Fig. 3. General tectonic structure of the Dead Sea Basin. The major faults and the location of the Lisan and Sedom diapirs are shown (ten-Brink & Ben-Avraham, 1989; Kashai & Crocker, 1987; Neev & Hall, 1979). Depth cross-section along the axis of the basin, which was based on gravity modeling, is shown in the left side of the map of the basin (ten-Brink et al., 1993). Coordinates are in Cassini Palestine grid.

NRA1 and NRA 3, Ghor Safi-1). In order to define the corresponding reflectors on all seismic lines, we correlated the stratigraphic units with the closest seismic lines, and extended the correlations to tie lines farther away. In particular, the interpretation of the various seismic horizons on lines 632 and line A, (Figs. 6 and 7) is based on correlation with borehole information (e.g. Gardosh et al., 1997). The interpretation of seismic lines B, 1, 3A, and 7, (Figs. 7–10) is based on correlation of two-way travel times and the characteristics of specific reflectors with the above lines, because boreholes in the Lisan Peninsula only penetrated through a thin layer of Lisan marl into the Pliocene salt, but

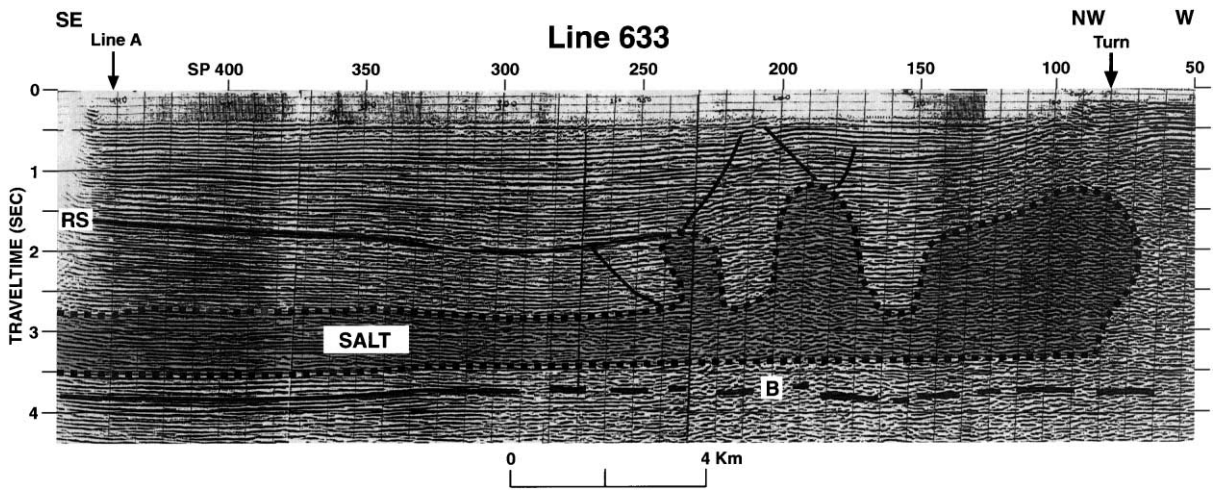

Fig. 4. Seismic line 633. The dashed lines show the top and bottom of the salt body (shaded). Horizon B — interpreted top of the pre-rift sediments. Horizon RS — Interpreted base of a salt withdrawal basin (rim syncline). Dark black lines — faults.

never reached the bottom of the salt. Ghor Safi 1 and Numeira 1 boreholes south of the Lisan Peninsula never reached the Pliocene salt (Al-Khalidi, Abu Ayyash, Al-Nabulsi, & Sabha, 1997). In addition, there was no reliable velocity information from these boreholes. Three horizons were identified on all the profiles: top salt, bottom salt, and the top of pre-rift (pre-Miocene) sediments.

The Sedom Deep 1 and Amiaz East boreholes show that the southern Dead Sea basin fill consists of three main units (Fig. 2; Gardosh et al., 1997). The basal unit, referred to as Hazeva Formation, was deposited in fluvial and lacustrine environments during the Middle and Late Miocene. This main clastic unit consists mainly of quartz sandstones derived mostly from distant sources south and east of the basin. It is characterized by coherent strong amplitude reflections in the seismic reflection profiles and is more than 1650 m thick in Sedom Deep 1 borehole.

The middle unit is a Late Miocene to Pliocene salt layer with a variable thickness. Where deformed, such as in salt diapirs, the reflectors are chaotic. Away from the diapirs, the layer can be reflective (e.g. Figs. 5–7). It is 900 and 1300 m thick at Sedom Deep-1 and Amiaz East boreholes, respectively (Gardosh et al., 1997). The upper part of the basin is filled with Pleistocene–Holocene sediments that are more than 4 km thick in some places. This unit consists of marl, clay, sand, gravel and some evaporites deposited in fluvial

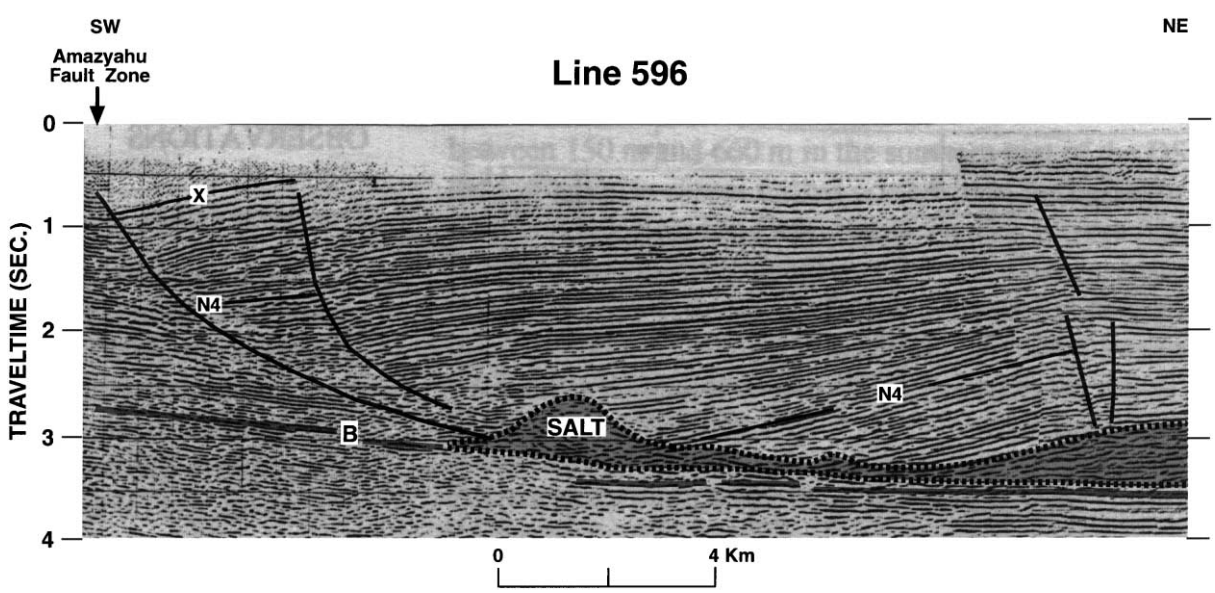

Fig. 5. Seismic line 596. The dashed lines show the top and the bottom of the salt body (shaded). Horizon B — interpreted top of the pre-rift sediments. Horizon N4 — interpreted sequence boundary within the Pleistocene sediments. Horizon X — tilted shallow reflector indicating continued extension on the Amazyahu Fault in recent times. The Amazyahu fault zone is shown in the southwest end of the line, as a listric fault, which extends to a depth of about 3.3 s. The subhorizontal portion of the fault plane probably soles into the Pliocene salt layer.

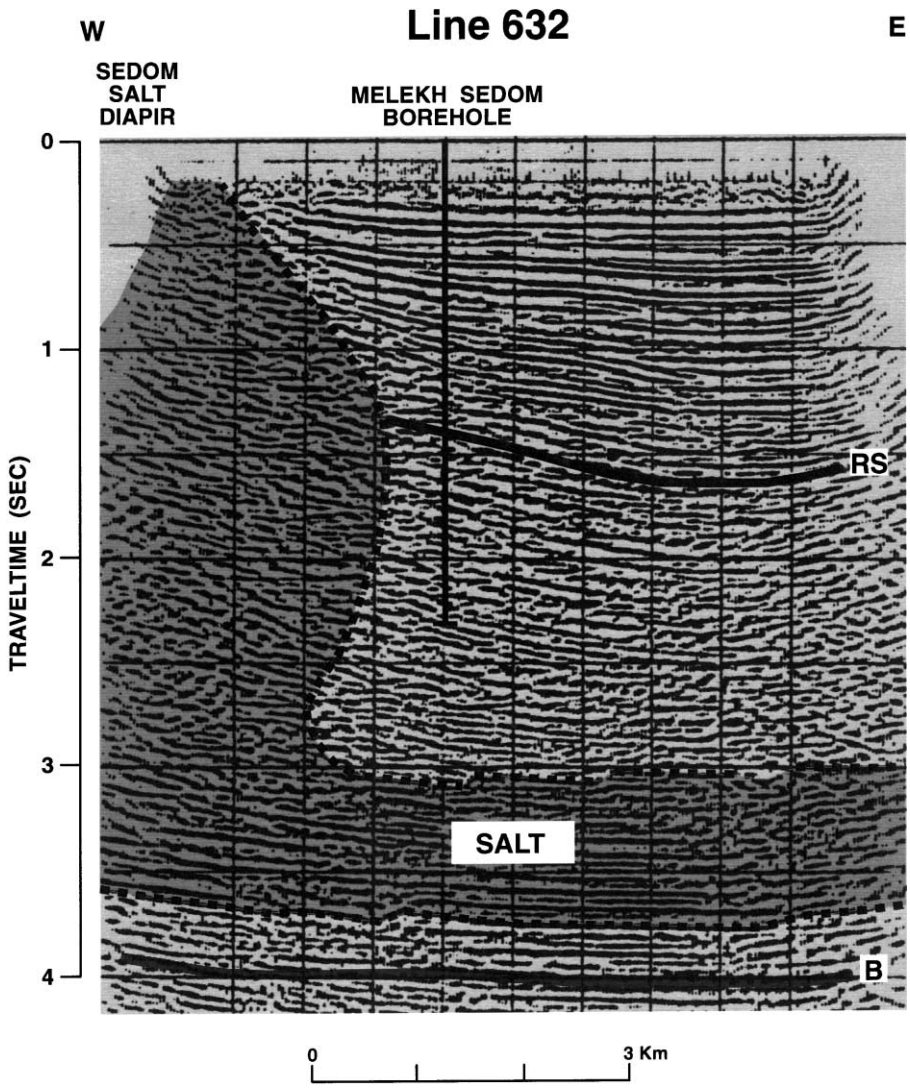

Fig. 6. Seismic line 632. The dashed lines show the top and the bottom of the salt body (shaded). Horizon B — interpreted top of the pre-rift sediments. Horizon RS — interpreted base of a salt withdrawal (rim) syncline.

and lacustrine environments. In the central block, 3870 and 2783 m have been penetrated in Sedom Deep 1 and Ghor Safi 1, respectively. The Pleistocene sequence appears on the seismic section as a series of subparallel high and low amplitude and frequency reflections that extends to a maximum depth of 3.0 s TWT (e.g. Fig. 6).

The Pleistocene layers were deformed around the growing diapirs. Syn-depositional deformation in some lines (e.g. Figs. 8 and 10) indicates that the salt diapir (Lisan diapir) is still growing episodically as evidenced by sediment onlap onto reflectors A1 and A2 (Fig. 8). On the eastern flank of the Sedom diapir, the entire Pleistocene section from about 1.2–3.0 s is inclined (Fig. 7), suggesting that in this area, salt flowed continuously westward and upward from the deep basin throughout the late Pleistocene (Gardosh et al., 1997). Diapiric growth could actually have been downward, because the strata flanking the diapers probably sank as much as or even more than the diapir rose relative to the geoid (Barton, 1933). West of the Sedom diapir, the young sedimentary fill shows very little deformation (Fig. 7; Gardosh et al., 1997), except adjacent to the diapir where layers are curved by contact drag. Sediments away from the edges of both diapirs (Lisan and Sedom) have subsided to form salt-withdrawal basins or rim synclines (a reflection event that emphasizes the subsidence of the rim syncline is marked by RS in Figs. 4, 6–8 and 10). The extent of the subsidence is probably indicative of the area from which salt has been withdrawing to supply the rising diapir (Alsop, 1996; Seni & Jackson, 1983; Trusheim, 1960).

The deformation associated with the edge of the salt (SP 200–250 in Fig. 4) was previously interpreted as a diagonal fault within the basin fill, the Boqeq Fault, (Fig. 3) crossing the Dead Sea basin in a NW–SE direction (Ben-Avraham et al., 1990). This interpretation was based on analysis of a single line (Fig. 4) and the observation of a NW–SE zone

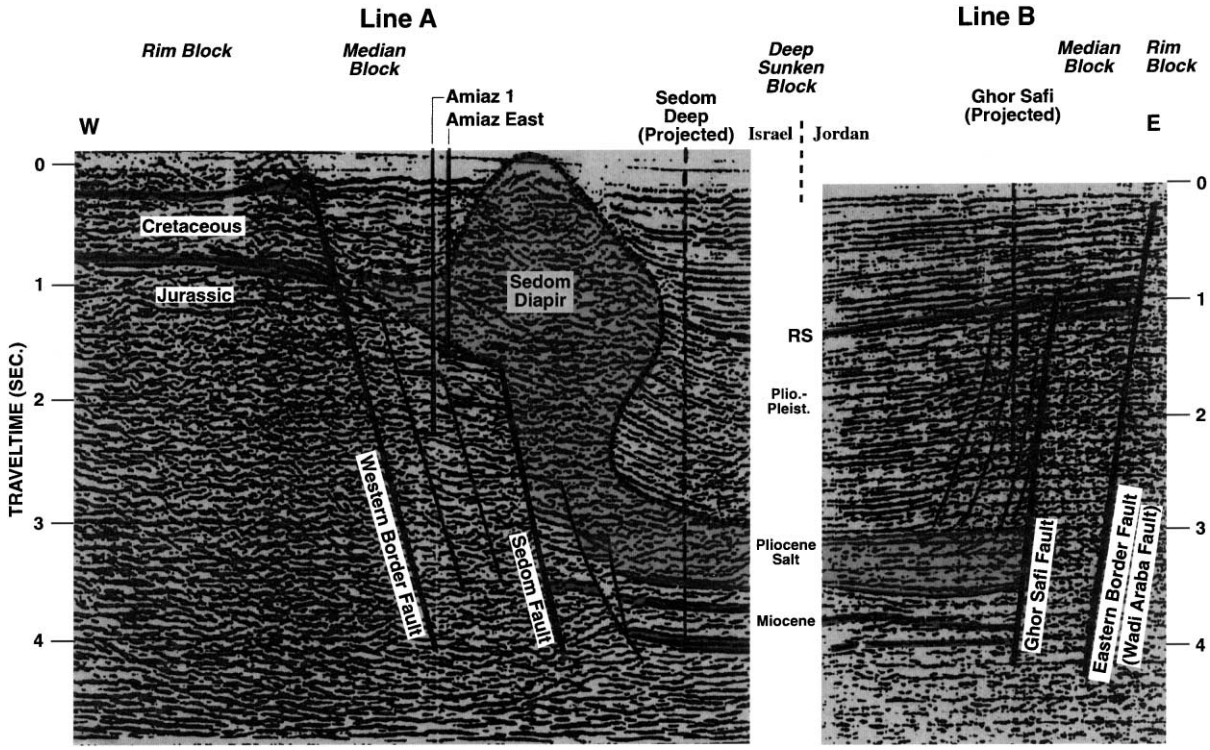

Fig. 7. Seismic lines A and B (Al-Zoubi et al., 2001) showing the main structural elements on both sides of the southern Dead Sea basin: Rim Blocks, Median Blocks, Deep Sunken Block and the faults that separate them. The location of Sedom Deep 1 well is projected into line A. Horizon RS — interpreted base of a salt withdrawal (rim) syncline.

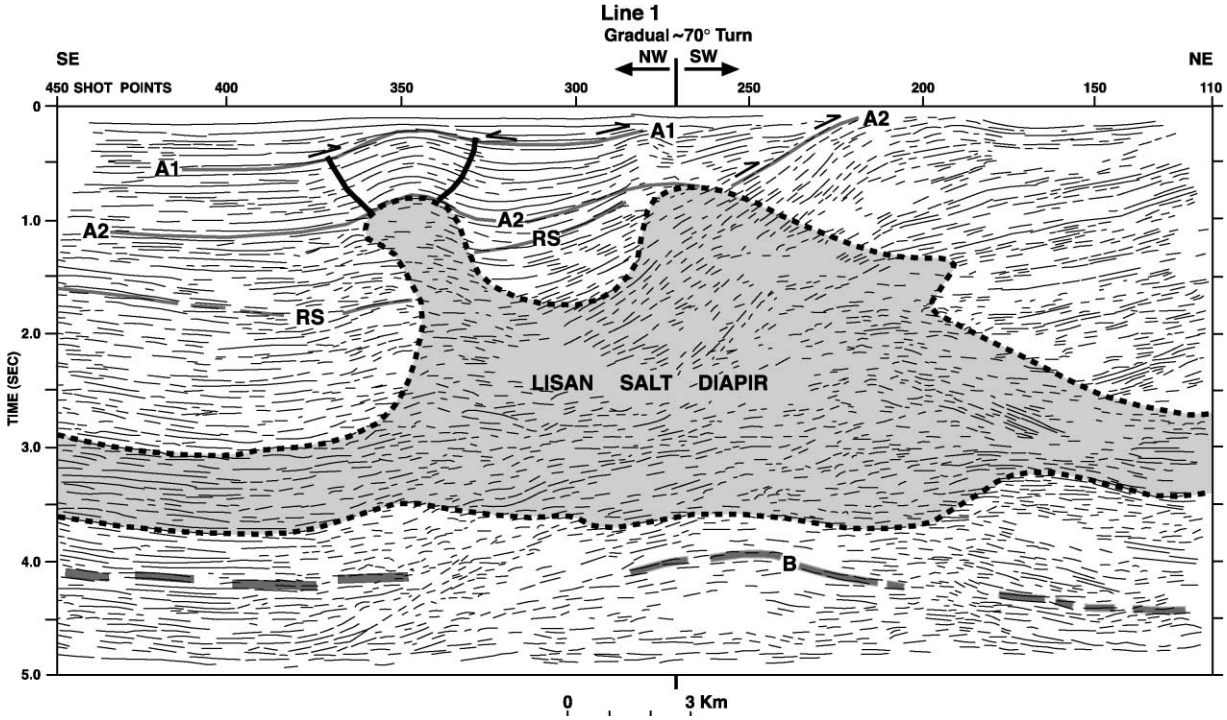

Fig. 8. Line drawing of seismic line 1 showing the northwestern and southwestern edges of the Lisan diapir. Note a gradual ~70°-turn of the line orientation from northeast to southeast (see Fig. 1 for location). Horizons A1 and A2 — Onlap surfaces indicating onlap of basin fill on the deforming edge of the Lisan diapir. Other symbols as in previous figures.

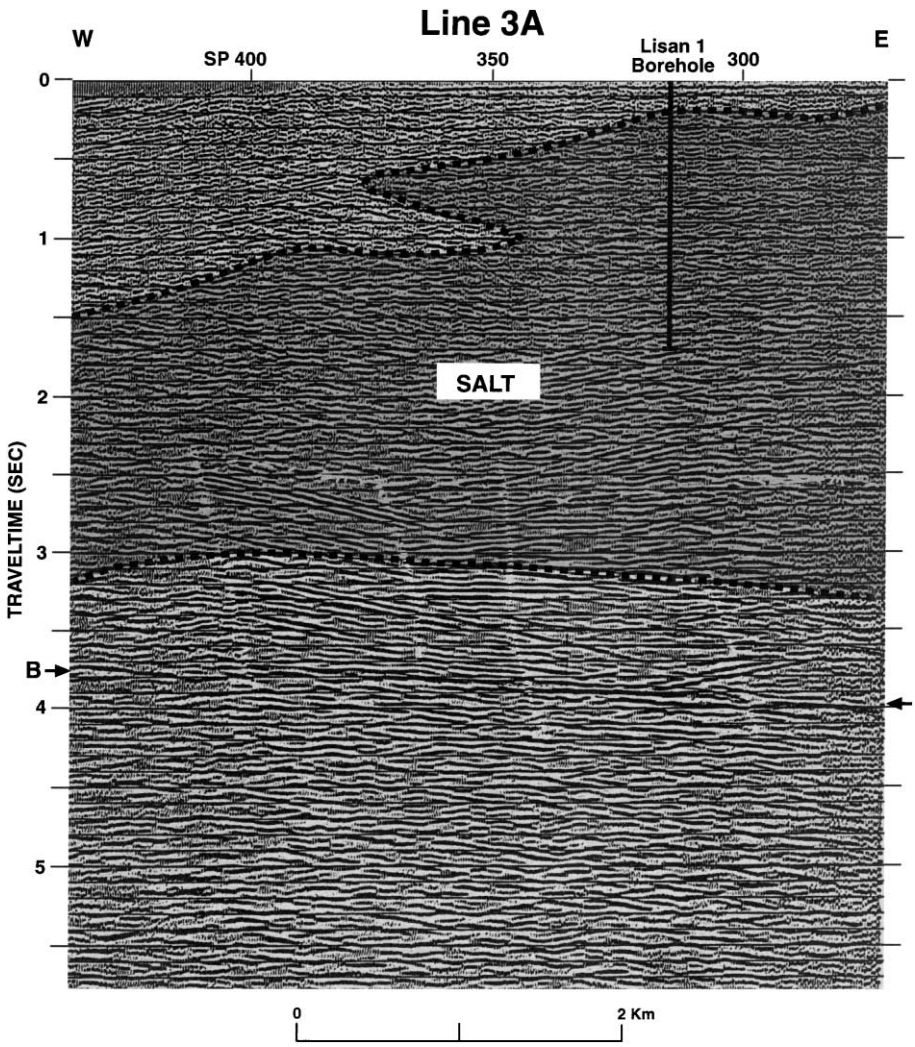

Fig. 9. Seismic line 3A crossing the western half of the Lisan diapir. The dashed line shows the top and the bottom of the salt body (shaded). Horizon B between two arrows — interpreted top of the pre-rift sediments. The location of the Lisan 1 well is shown.

of deformation on very high-resolution seismic data west of Line 633. Based on the additional subparallel seismic profiles presented here, we now believe that this deformation represents the edge of a salt diapir, rather than a fault in the basin fill. In particular, seismic line 7 (Fig. 10) running in the N–S direction farther east should cross the proposed Boqeq fault (Ben-Avraham et al., 1990), but shows no evidence for an E–W crossing fault. The boundary between the zones of coherent reflectors and chaotic reflectors in this profile is steep or overhanging, which is typical to an edge of many salt diapirs. This boundary is located NE of the proposed location of Boqeq Fault on Line 633, not SE, as predicted by a diagonal fault. Line 1 (Fig. 8) which runs parallel to Line 633 about 1 km to the east shows more clearly than line 633 the salt deformation of the overlying sediment. We interpret lines 1 and 633 to cross the southwest corner of the Lisan diapir. The patches of coherent reflectivity north of the previously assumed location of Boqeq Fault in Lines 1 and 633 are interpreted to be regions where the seismic profile grazed in and out of the undulating edge of the diapir. Inspection of additional lines (e.g. line 8 and 2D, see Figs. 12 and 13 for location) precludes the presence of another diagonal fault south of the previously assumed location of Boqeq Fault. Thus, we suggest that contrary to previous interpretations (Ben-Avraham et al., 1990), there is no major diagonal fault cutting the Pleistocene section between the Sedom and Lisan diapirs. We cannot determine from the seismic reflection lines whether diagonal faults are present below the base of the basin fill.

3.2. Horizon depth maps

The seismic profiles were used to construct depth maps to three horizons, top of Pliocene salt, bottom of Pliocene salt, and the base of the rift-fill sediments. In order to create these maps, we converted two-way travel times in the seismic profiles to depth using sonic information from Sedom Deep 1 well (Fig. 2). The sonic log indicates that velocity increases with depth. It is on average 2.5 km/s for the first 1.2 s TWT, 3.5 km/s for the lower part of the Pleistocene

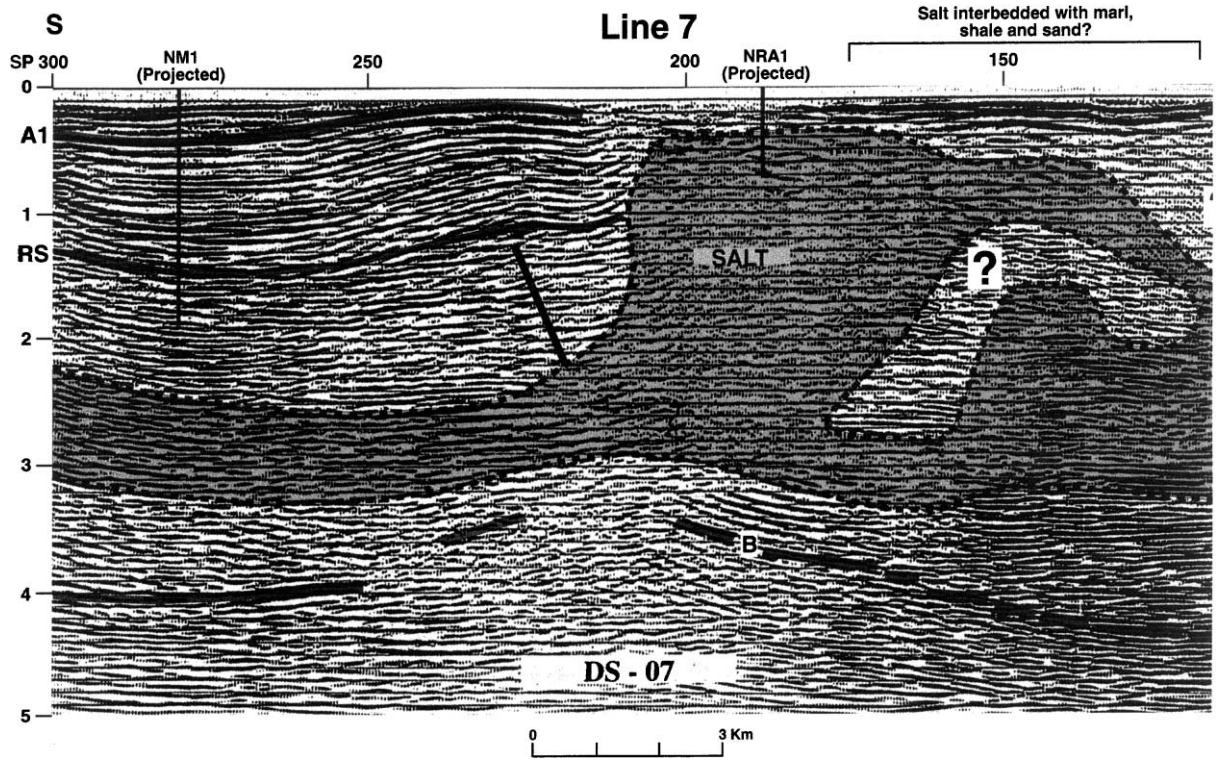

Fig. 10. Seismic line DS7. The line crosses the Lisan diapir in a north–south direction. We interpreted patches of reflectivity within the salt diapir (marked by ?) as salt interbedded with marl, shale and sand. The reflective patches may be showing because the seismic profile runs along the eastern edge of the diapir, which is undulating. Black line — fault. Other symbols as in previous figures.

sediments, 4.3 km/s for the Pliocene Sedom salt, and 4.5 km/s for the Miocene Hazeva Formation.

The top of the salt in the study area forms two anticlines. The largest one is located in the Lisan Peninsula (Lisan diapir) and the second one the Sedom diapir, along the southwest longitudinal fault (Fig. 11). The top of the Lisan diapir extends farther to the south than previously mapped (e.g. Neev & Hall, 1979) but is deeper in the northern and westernmost edges of the Lisan Peninsula. The top of the diapir is encountered at a depth of about 125 m in Lisan 1 borehole. In contrast, the elongate Sedom diapir rises up to 200 m above the basin floor. Fig. 11 shows the top of the salt between the two diapirs and farther east and south at a depth of 4500–5000 m. The only exception is the area immediately SE of the Lisan diapir where the top of the salt is shallower.

The salt layer beneath the Pleistocene sediments ranges in thickness (in TWT) from 0.4 s in the southern part of the study area to more than 3 s in the Lisan Peninsula, which corresponds to a thickness range between 900 and 7000 m, respectively. The lower boundary (bottom) of the salt in the majority of the seismic profiles is relatively flat, except at the edges of the Lisan and Sedom diapirs. The bottom of the salt reaches a maximum depth of 7250 m under the Lisan diapir. The area connecting the two diapirs is relatively flat with the bottom of the salt layer located at a depth of about 5750 m (Fig. 12). These estimates are probably accurate to within 250 m, because an uncertainty of ± 0.1 s in the identification of the bottom of the salt layer, contributes to a depth uncertainty of ± 215 m.

The structural map of top pre-rift sediments (Fig. 13) (pre-Miocene), which is equivalent to the base of the Hazeva Formation of fluvial and lacustrine deposits, is generally similar in shape to the structural map of the bottom of the salt. The depth to the pre-rift sediments in the study area increases from the south (about 6.5 km) to the north where it reaches a depth of about 8.5 km and forms a low structure under the eastern Lisan Peninsula. The top of prerift sediments lies at a depth of about 6.25–7 km beneath the Sedom diapir. Sedom Deep 1 was drilled 1675 m into Miocene sediments, but did not reach pre-rift sediments when drilling terminated at a depth of 6445 m. The maximum depth of the basin under the Lisan peninsula, 8.5 km, is shallower than previously suggested on the basis of gravity modeling (10 km, ten Brink et al., 1993).

The structural map of the top pre-rift sediments also reveals the existence of a narrow median block, 2–3 km wide, along part of the eastern boundary of the Dead Sea (Fig. 13). Line B (Fig. 7), lines 2D and 8, line E, and line C (see Fig. 13 for location) show that this block extends only a limited distance along the eastern boundary of the basin, possibly, where the basin is the deepest. A more areally extensive median block was previously identified along the western boundary of the basin (Kashai & Crocker,

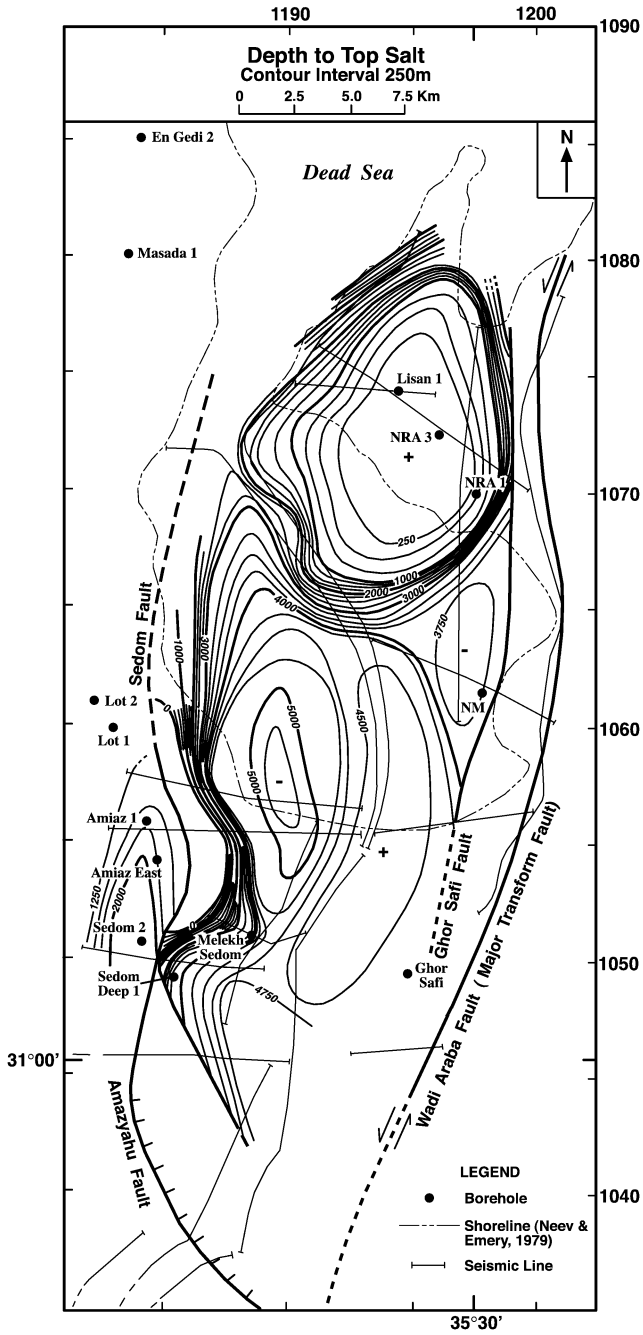

Fig. 11. Depth to top salt map. The contour interval is 250 m. Two anticlinal structures, Lisan and Sedom Diapirs, are shown. The location of all seismic lines, used for the analysis and the well location are shown. Line numbers are given in Fig. 13. Depth refers to depth below local surface (−400 m). See text for discussion on travel time conversion to depth.

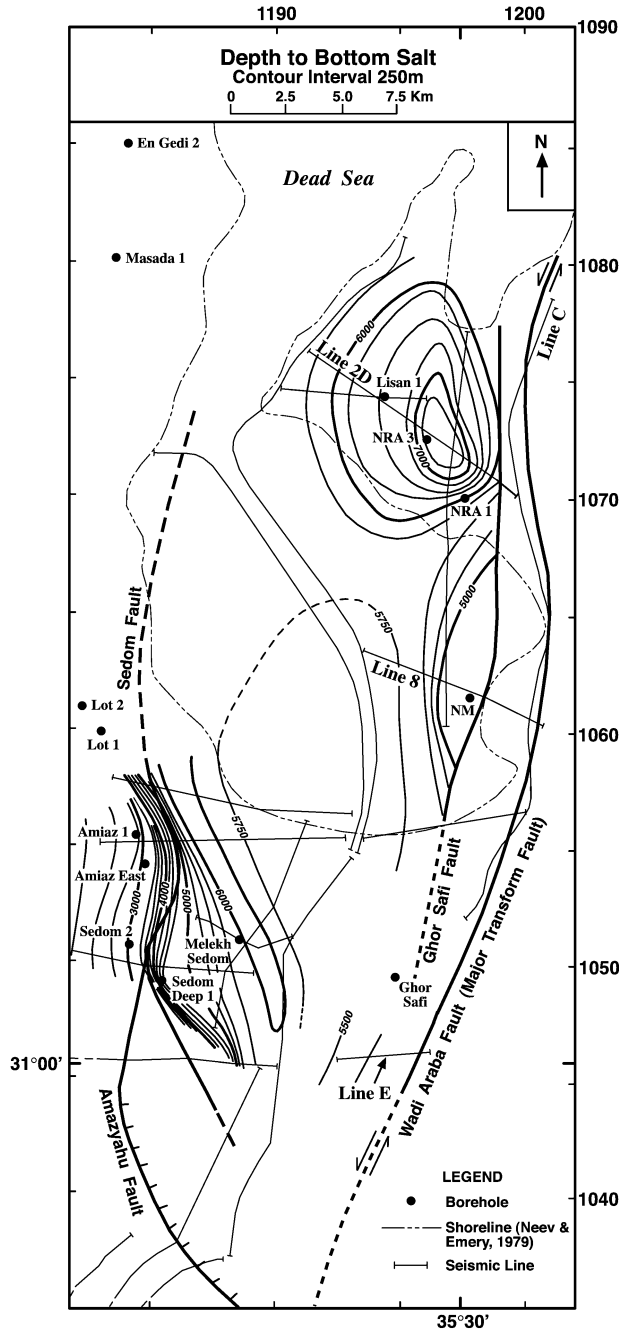

Fig. 12. Depth to bottom salt map. Contour interval 250 m. See Fig. 11 for more information.

1987) and was attributed to the collapse of the basin wall (ten Brink et al., 1993).

3.3. Gravity modeling

Gravity modeling was used to check the seismic interpretation of the extent and depth of the Lisan salt diapir. The gravity data in the study area (Fig. 14) were collected by the Natural Resources Authority of Jordan (NRA) and the Geophysical Institute of Israel (GII), and during a marine survey of the Dead Sea in 1988 (ten Brink et al., 1993). A joint database of gravity measurements for Jordan and Israel was established by NRA and GII and the US Geological Survey (ten Brink, Rybakov, Al-Zoubi, Hassouneh, Bataynrh, Frieslander et al., 1998, 1999), and has since been updated periodically. Two Bouguer gravity profiles were extracted from this data base, a 25 km-long profile across

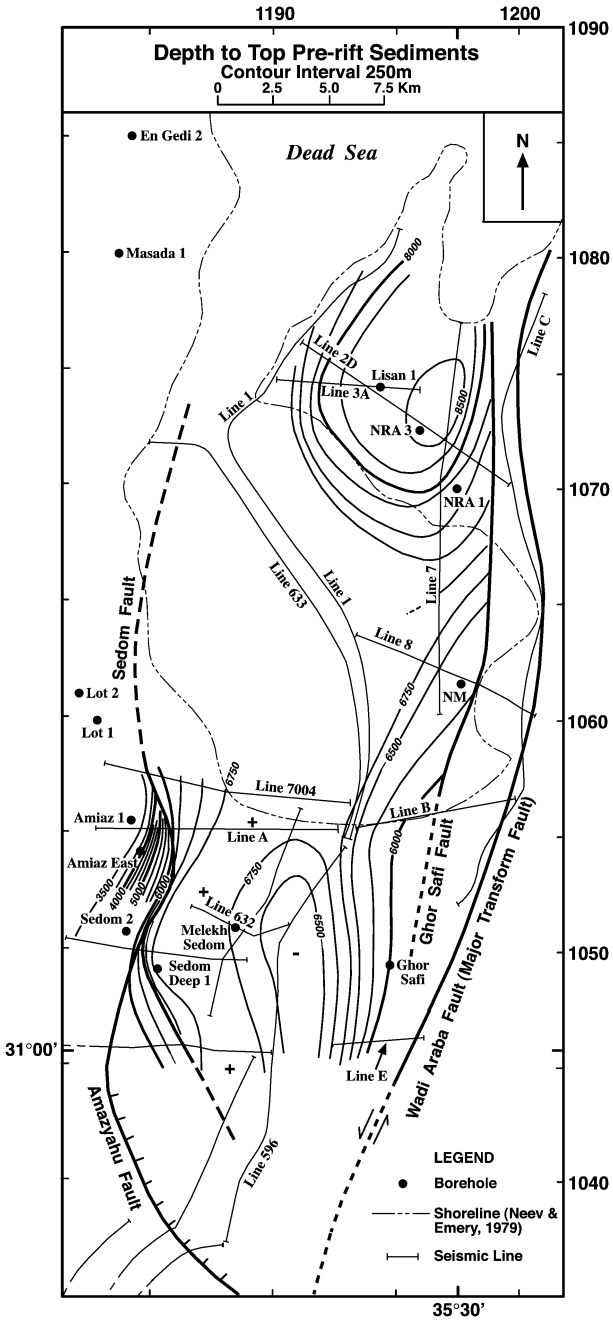

Fig. 13. Depth to top pre-rift sediments map. Contour interval 250 m. See Fig. 11 for more information.

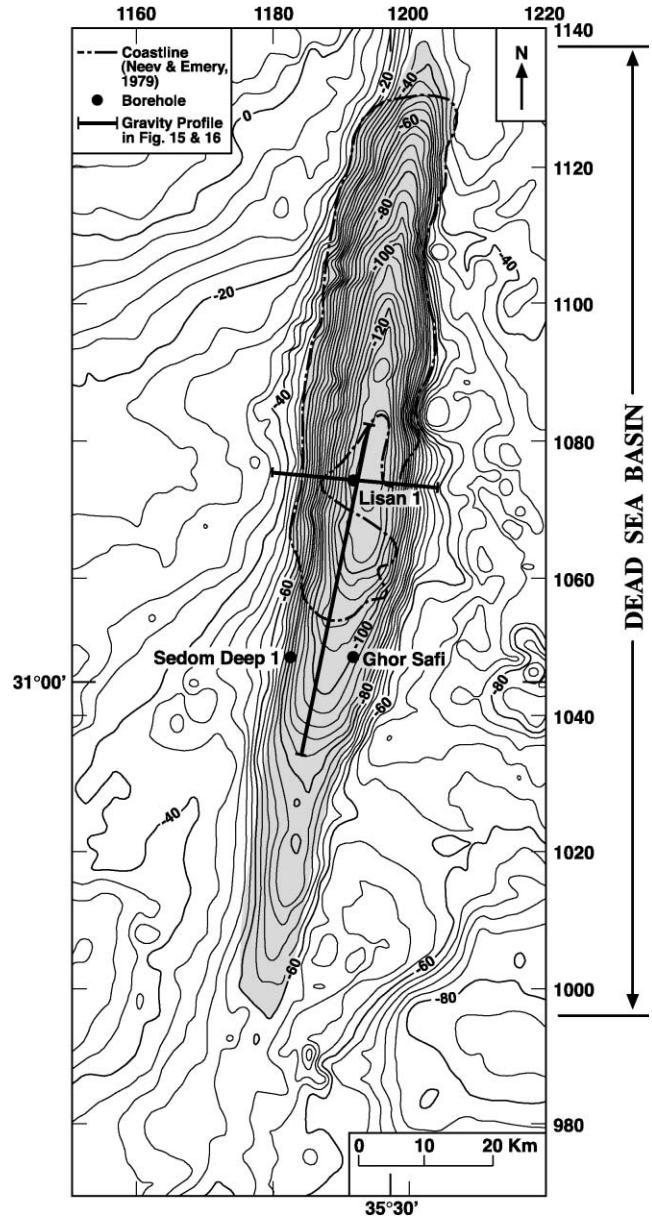

Fig. 14. Bouguer gravity anomaly map of the study area. Contour interval is 3 mGal. Location of the gravity profiles in Figs. 15 and 16. Dashed-dotted line — 1967 coastline of the Dead Sea (after Neev & Hall, 1979). Black dots — location of wells.

the basin and a 50 km-long profile along the basin (Fig. 14 for location). Two-dimensional gravity models (Figs. 15 and 16) were constrained by the structural maps derived from the seismic reflection profiles. Density values for the upper part of the sections were derived from the density well logging carried out in Sedom Deep-1 (Rybakov, Goldshmidt, Fleischer, Rotstein, & Goldberg, 1995a). Densities of pre-rift sediments and the crystalline crust were derived from borehole data in the surrounding areas of Jordan and Israel and from samples collected in the southern part of Jordan (Abu-Ajamieh, 1967). The fit between the observed and calculated gravity values was found to be satisfactory and the standard deviation of the differences is 2–3 mGal.

The Lisan salt diapir reaches a maximum depth of 7.2 km on the east–west profile (Fig. 15), but is slightly less deep on the north–south profile (Fig. 16) because that profile is located west of the maximum depth of the diapir across Lisan-1 borehole (Fig. 12). The salt body is thinner on the west side of the basin, and its base depth of 5.5 km is similar to the depth to the bottom of the salt farther south. The north–south profile indicates an abrupt thinning of the salt body to the south is also as seen on Fig. 10. The termination

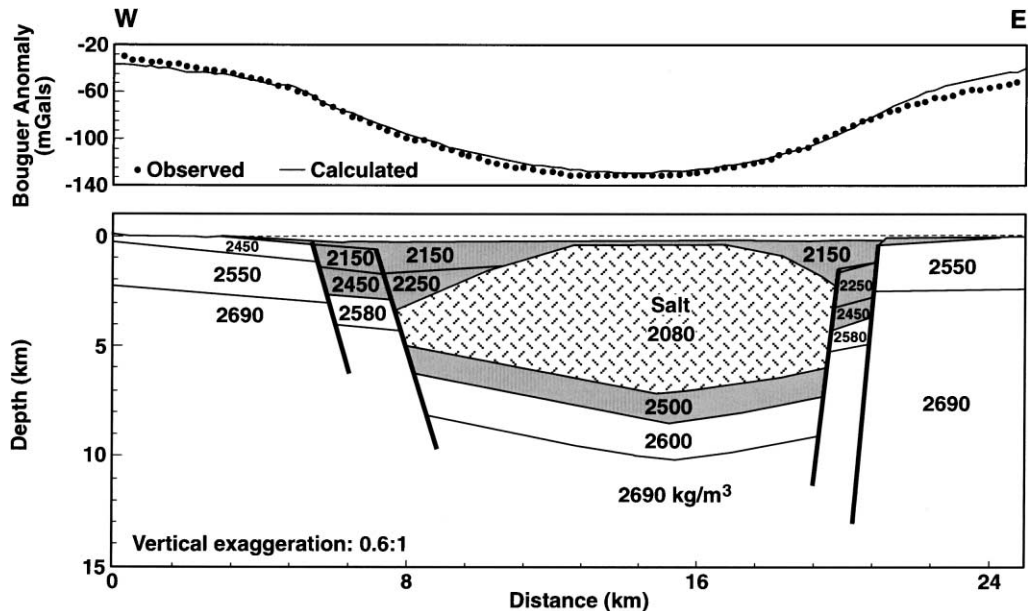

Fig. 15. An observed and calculated gravity profile over the Lisan Peninsula running partly along seismic line 3A (Fig. 9). The shaded layers represent synrift sediments. The salt has a density of 2080 kg/m^3. The RMS difference between the observed and calculated gravity value less than 3 mGal.

of the salt body to the north is more gradual according to the gravity model.

Crystalline basement with a density of about 2690 kg/m^3 is estimated to be at a maximum depth of 9.5–10.5 km under the Lisan diapir. The thickness of the overlaying Paleozoic and Mesozoic sections are about 1.5–2 km estimated from geological cross-sections east and west of the basin, and their average density is 2600 kg/m^3 (Abu-Ajamieh, 1967; Rybakov, Goldshmidt, Rotstein, Fleisher, & Goldberg, 1999). The Miocene sequence has a density of 2500 kg/m^3 (Fig. 2) and is about 1750 m thick (Gardosh et al., 1997). The overlaying Pliocene salt and Pleistocene series are about 7 km thick under the Lisan and 5.5–6 km thick farther west and south. The density for the salt body, 2080 kg/m^3, was taken as the average density between the Sedom Deep-1 density log (2150 kg/m^3, Rybakov et al., 1995a) and the Numeira density log (1960 kg/m^3, Qabbani, pers. commun., 2000). We divided

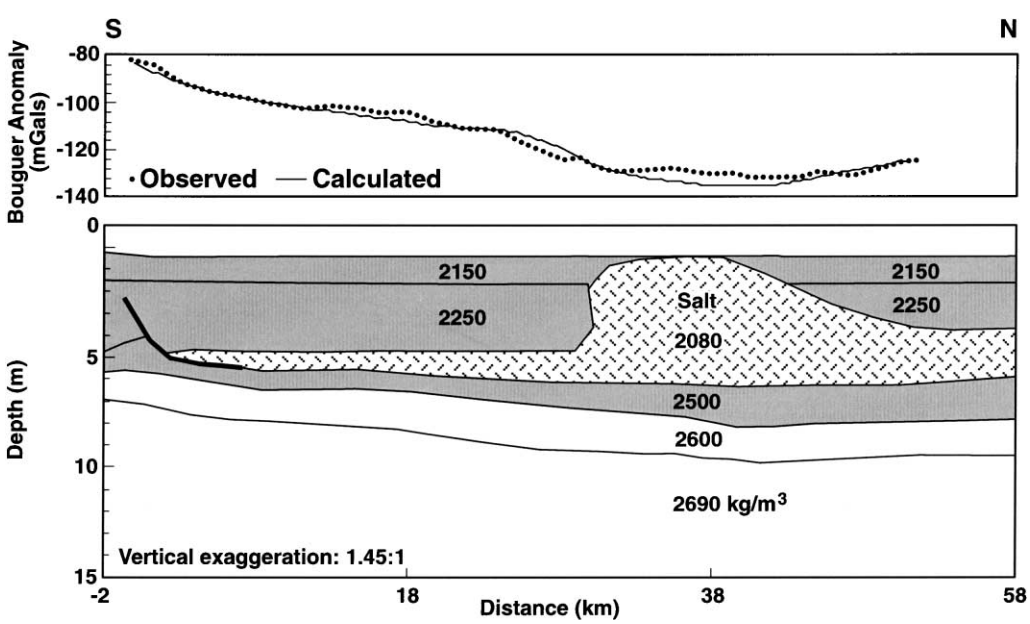

Fig. 16. An observed and calculated gravity profile over the Lisan Peninsula running in the N–S direction. The shaded layers represent synrift sediments. The salt has a density of 2080 kg/m^3. Heavy black line — Amazyahu fault. The RMS difference between the observed and calculated gravity value less than 3 mGal.

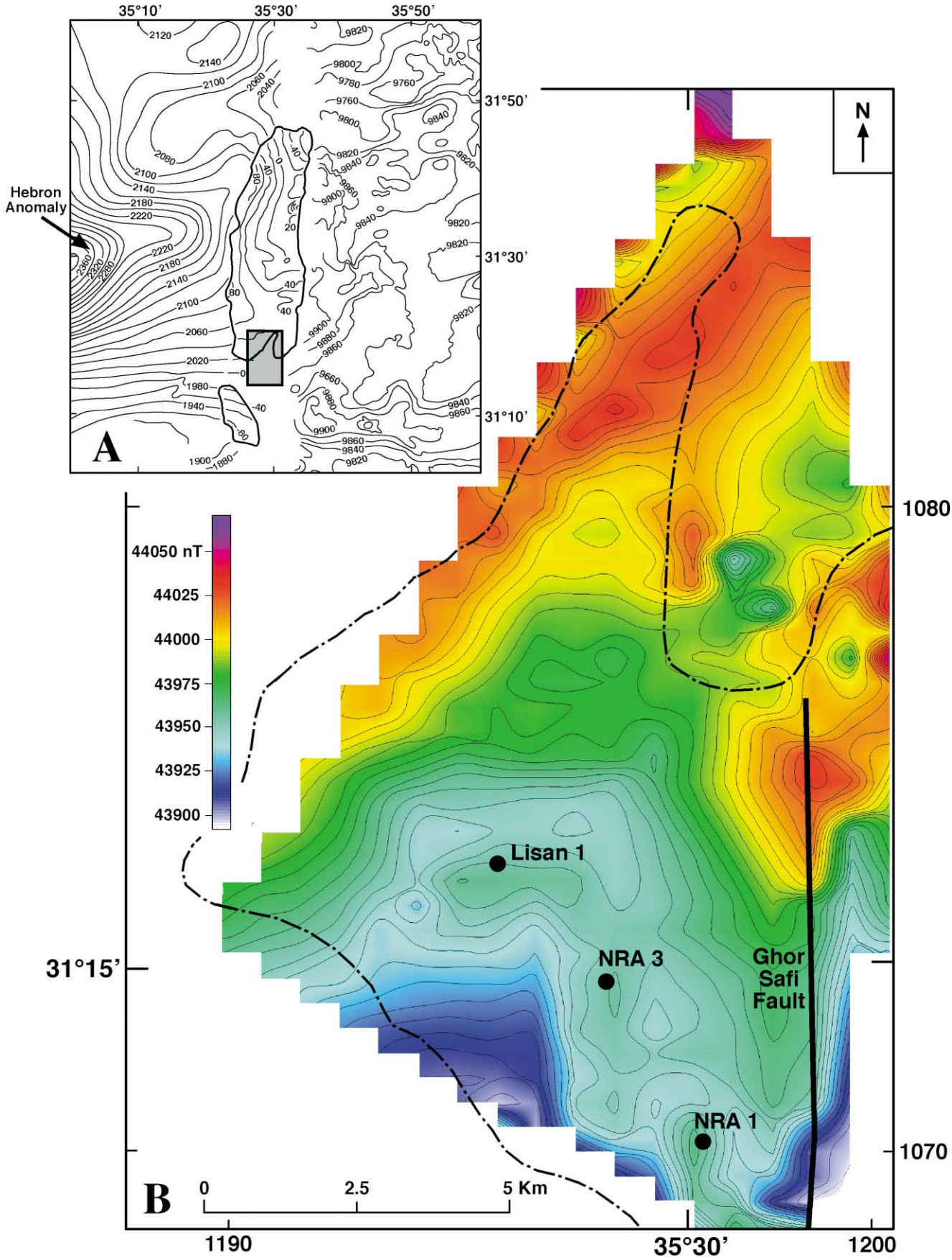
35°10'
35°30'
35°50'
31°50'
31°30'
31°10'
Hebron Anomaly
A
N
44050 nT
44025
44000
43975
43950
43925
43900
Lisan 1
NRA 3
NRA 1
Ghor Safi Fault
31°15'
1080
1070
B
0
2.5
5 Km
1190
35°30'
1200

the Pleistocene sediments into a lower part with a density of about 2250 kg/m^3 and an upper part above 1.5–2 km with a density 2150 kg/m^3.

3.4. Magnetic data

Magnetic data help delineate the areal extent of the Lisan diapir and the location of the Ghor Safi Fault. Several magnetic studies have been carried out previously in the Dead Sea and surrounding areas (Frieslander & Ben-Avraham, 1989; Neev & Hall, 1979; Ram, 1989), but none of them covered the Lisan Diapir. Larger scale aeromagnetic surveys of the surrounding highlands (Folkman, 1976, 1981; Hatcher, Zietz, Regan, & Abu-Ajamieh, 1981; Fig. 17A) provide the regional shape of the magnetic field. These data were combined in a joint magnetic database of Jordan and Israel that was established at the Natural Resources Authority. Here we present new results of a recent ground magnetic survey carried out by NRA on the Lisan Peninsula (Al-Zoubi, 2000) (Fig. 17B). The magnetic measurements were taken by NRA along about 220 km of track roads opened by Arab Potash Company and NRA. The magnetic survey lines were oriented S–N and W–E. A proton magnetometer G-856 with an accuracy of 1 nT was used. The magnetic values were corrected for the diurnal variations and a total magnetic field map with a contour interval of 5 nT was generated (Fig. 17B).

A smoothed low anomaly is observed over the southern part of the Lisan Peninsula, whereas the northern and eastern parts are characterized by shorter wavelength anomalies. We interpret the smoothed anomaly to reflect the location of the Lisan diapir at shallow depths beneath the surface (Compare with Fig. 11). The discontinuity of the magnetic anomaly in the eastern side of the Dead Sea rift is interpreted to indicate major lithologic changes across the Ghor Safi fault.

The total magnetic map (Fig. 17A) shows an overall north-to-south gradient of 185 nT in the magnetic field intensity recorded over a distance of about 17 km, giving a horizontal gradient equal to 10.8 nT/km. The magnetic map of the Dead Sea and surrounding areas (insert in Fig. 17A; Ben-Avraham, 1997), shows that the regional magnetic field decreases from the north to the south. Thus, the gradient likely reflects the regional field. The regional field is dominated by a large magnetic anomaly centered about 40 km west of the Lisan. The anomaly, referred to as the Hebron anomaly, is thought to represent a large buried Jurassic intrusive body (Rybakov, Fleischer, & Goldshmidt, 1995b).

4. Discussion

The average dimensions of the Lisan diapir according to our interpretation of the salt dome in seismic profiles are about 13 km by about 10 km with an average thickness of 6 km. These dimensions give a salt volume of 780 km^3. The Sedom diapir has only one-tenth of the salt volume of the Lisan, 68 km^3 (11 km length, 1.25 km wide, and 5 km thick). If the salt withdrew from an area extending from Amazyahu fault in the south to the north edge of the Lisan diapir (an area of 65 km by 12 km minus the area of the diapirs), then the thickness of the withdrawn salt is on average 1.33 km. (As discussed earlier, the extent of a salt layer north of the Lisan is not well known.) The average thickness of the Pliocene salt outside the diapirs is 0.9–1 km (Figs. 11 and 12; Gardosh et al., 1997; Kashai & Crocker, 1987), hence the original salt thickness was close to 2.3 km, similar to the estimate by Garfunkel (1997). It indicates that the basin had subsided by at least that amount during the Pliocene.

Fig. 12 shows that the base of the Lisan salt diapir is deeper than the average depth to bottom of salt between the two diapirs and therefore is below the base of the salt layer from which the salt withdrew. If subsidence had occurred during the development of the diapir, both the subsidence and the development of the diapir may have resulted from extension within the basin. Vendeville and Jackson (1992a) argued that wherever the overburden extension is decoupled from basement extension by thick salt, a diapir will develop within the overburden. The development of the Amazyahu diagonal fault over the salt layer indeed indicates that overburden extension was decoupled from a north–south basement extension during the development of the pull-apart basin in the Pleistocene (Fig. 5; ten Brink & Ben-Avraham, 1989).

Given a constant salt thickness, diapirs will develop where the overburden was thinned relative to the surrounding tabular area (Fig. 18), provided the viscosity of the salt is not too great to resist the flow and that synkinematic sediments do not infill the graben too rapidly (Vendeville & Jackson, 1992a). The overburden in the Dead Sea basin is made of Pleistocene unconsolidated lacustrine and fluvial sediments (Fig. 2). Physical models show that the rate of reactive diapiric rise is controlled by the rate of basin extension during the 'reactive stage' of diapir development, i.e. before the overburden is sufficiently thin to be completely pierced by the diapir (Vendeville & Jackson, 1992a). We, attribute the initiation of the Lisan diapir to north–south directed extension that caused local subsidence in the Lisan area during the Pleistocene and resulted in this area being 1.5–2 km deeper than the surrounding area. This

Fig. 17. (A) Magnetic anomaly map of the Dead Sea and its vicinity (Ben-Avraham, 1997). Contour interval is 20 nT. The map shows different values east and west of the Dead Sea because they represent three separate aeromagnetic surveys (Folkman, 1976, 1981; Frieslander & Ben-Avraham, 1989; Hatcher et al., 1981) flown at different times and at different elevations. Solid line — 1987 coast line. (B) Total magnetic field map of the Lisan Peninsula from recent land measurements Al-Zoubi, 2000). Contour interval is 5 nT. Dashed-dotted line — 1967 coast line. Filled circles — Location of boreholes.

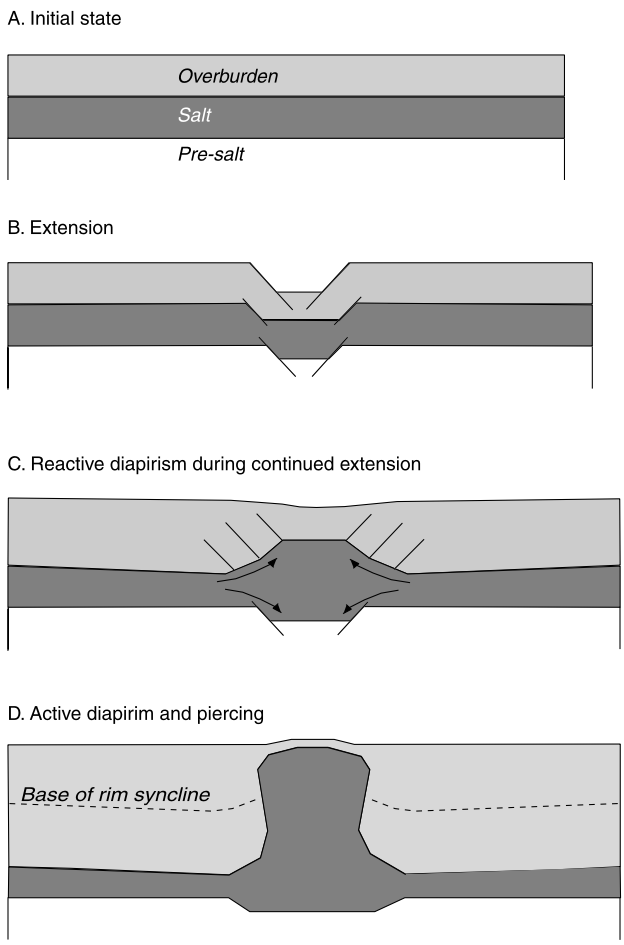

Fig. 18. A conceptual model for the development of the Lisan Diapir during the Pleistocene. Stages B and C were separated for the sake of illustration but are effectively one continuous stage. This model does not include possible recent periods of lateral compression and renewed diapiric rise. See text for further details.

subsidence may be similar to the recent local subsidence farther north within the Dead Sea (Neev & Hall, 1979). Some buried faults, shown in Figs. 4 and 10, may be remnant faults from the overburden extension.

The next stage in diapir development, the active stage, occurs when the fluid pressure at the crest of the diapir becomes sufficiently large to lift and move aside the thinned overburden. At this point, the diapir rises rapidly and pierces the surface (Vendeville & Jackson, 1992a). Continued upward flow is controlled by the buoyancy and the rate of supply of the salt rather than by regional extension (Vendeville & Jackson, 1992a) In fact, if regional extension continues, and salt supply becomes restricted, the diapir would start subsiding to fill the additional room created by extension (Vendeville & Jackson, 1992b). In addition, if the rates of downward dissolution of the salt or sediment accumulation in the basin are higher than the upward salt flow, the diapir will eventually be buried (Vendeville & Jackson, 1992b). We interpret the Lisan diapir to be at this stage, because more than 125 m of Lisan marl covers the diapir. Continued N–S extension along the Amazyahu Fault, as seen in Fig. 5, would retard the upward flow of the Lisan Diapir. Fig. 18 summarizes our conceptual model for the development of the Lisan diapir.

A closer look at the topography and at the stratigraphy around the Lisan diapir shows, however, a more complex diapiric growth than described above. The Lisan Peninsula rises up to 50 m above the basin surface to the south, west, and east, suggesting that the diapir continues to rise. Onlap surfaces, marked A1 and A2 on Fig. 8, indicate two deformation phases along the western edge of the Lisan diapir. Shortening of the roof and flanks of the diapir may indicate two pulses of activity, possibly due to orthogonal compression. The earlier pulse occurred when the diapir was at or near the surface. A period of tectonic quiescence followed, in which the diapir was buried by up to 500 ms of sediments. The upper onlap surface records (Figs. 8 and 10) indicate the start of a second period of activity, which continues today. This renewed diapiric rise folded the isopachous layer between horizons A1 and A2 above the crest of the laterally squeezed, rejuvenated Lisan diapir.

If we accept the initiation of the salt diapers by extension, then sometimes during the Pleistocene, the area around the Sedom Fault was locally subjected to east–west extension. The E–W extension was probably a product of rapid basin deepening, which resulted in a large structural relief along the east and west boundaries of the basin. Monoclinal draping of the cover over these lateral steps could have created local E–W stretching and initiate a diapiric wall there. As discussed below, we believe that the reactive growing stage of the Sedom diapir coincided with the period of the most rapid subsidence. However, had E–W extension continued, the Sedom diapir would have eventually widened rather than growing taller. The diapir is still narrow and continues to rise, indicating little E–W extension, and perhaps even a local component of E–W compression. Continued rotation along the Amazyahu Fault may promote locally an E–W compression of the overburden along its northern continuation into the Sedom Fault, which will squeeze the diapir laterally. However, the main focus of basin subsidence is presently in the Dead Sea north of the Lisan (ten Brink & Ben-Avraham, 1989; Neev & Hall, 1979; Zak & Freund, 1981).

Diapir initiation is probably related to the tectonic evolution of the basin. At present, we can only suggest a relative time scale for the growth of the diapirs, because the Pleistocene section within boreholes in the area is not dated in detail. ten Brink and Ben-Avraham (1989) suggested that Amazyahu Fault initiated as a slide into the salt layer sometime during the early-to-Middle Pleistocene. Their suggestion is based on the observed thickening of the sedimentary section toward the fault above Reflector N4 (Fig. 5), which indicates that an accommodation space was developing by rotational fault slip at N4 time. Reflector N4 is about 2/3 down the Pleistocene section, and assuming

a constant sedimentation rate for lack of better constraints, it is dated as early-to-middle Pleistocene. The salt layer along the fault is tied with the salt that feeds the Sedom diapir (Gardosh et al., 1997) and the Amazyahu Fault itself curves northward toward the southern edge of the diapir (Fig. 11). It is thus possible that there is a genetic connection between the extensional faulting and the initiation of diapirism (Gardosh et al., 1997). The amount of overburden at the start of diapirism as represented by the sequence extending between the salt and reflector N4 in Fig. 5 is 0.8 s TWT, which corresponds to 1 km, assuming an uncompacted wave speed of 2.5 km/s. Comparison of the relative formation thickness between Amiaz East borehole on the median block and Sedom Deep 1 borehole in the deep basin (Gardosh et al., 1997) also suggests that the intervening Sedom Fault was particularly active during the lower-to-middle Pleistocene. The thickness of Lower-to-middle Pleistocene sequence on the median block is only 35% of that in the deep basin. In contrast, the relative thickness of the overlying upper Pleistocene formations (Samra and Lisan) in the median block is 65% of that in the deep basin, and the thickness of the underlying salt is actually larger on the median block than in the deep basin.

We can also map the salt withdrawal (or rim) synclines within the sedimentary section (e.g. Figs. 4, 6–8 and 10). Rim synclines are caused by salt withdrawal from around the diapir to supply salt into the diapir (Alsop, 1996; Seni & Jackson, 1983; Trusheim, 1960). The subsidence around the diapir, as evidenced by the rim synclines probably marks the time when diapiric growth became most vigorous (Alsop, 1996; Seni & Jackson, 1983; Trusheim, 1960). Diapiric growth is thought to be most vigorous during its active stage when the diapir is close to the surface or has pierced it and there is a large salt supply (Vendeville & Jackson, 1992a). Fig. 7 shows that subsidence started at around 1.2 s TWT, which assuming constant sedimentation rate, was in the middle-to-late Pleistocene, i.e. several hundreds of thousands of years after diapirism started. The rim syncline of the Lisan diapir is deeper, 1.5–2.1 s TWT (Figs. 4, 8 and 10), but still above reflector N4 (Fig. 5). It is conceivable that both diapirs may have started simultaneously, but the Lisan diapir may have developed more quickly into an active piercing diapir. This hypothesis is reasonable considering that the rate of diapiric rise in the reactive stage is determined by the rate of extension (Vendeville & Jackson, 1992a), and the north–south extension of the overburden in a pull-apart basin is much larger than that in the east–west direction.

The areal extent of the rim syncline is probably a good approximation to the source area for the diapir (Alsop, 1996; Seni & Jackson, 1983; Trusheim, 1960). In the Dead Sea basin, it shows that the entire basin area south of the Lisan and west of the Sedom diapir acted as a source region for the diapirs as we assumed earlier.

5. Summary and conclusions

The study uses newly released seismic reflection data from Jordan, published Israeli seismic data, gravity modeling, and a new magnetic map to delineate the extent and depth of the Lisan diapir. The Lisan diapir extends farther south than previously inferred, but its roof is deeper in the northern part of the Lisan than was previously assumed. The Lisan diapir extends to a maximum depth of 7.25 km, whereas the Sedom diapir and the salt layer south of the Lisan diapir are no deeper than 5.5–6 km. By constructing structural maps for the top and the bottom of the salt we can estimate the total volume of both diapirs to be 878 km^3, with 90% of the volume in the Lisan diapir. If the salt volume were supplied from a layer of salt spread evenly within a 65 km-long area, extending from the Lisan Peninsula to Amazyahu Fault, the thickness of that layer would have been 1.3 km. The present layer thickness is ~1 km suggesting that the original thickness of the salt layer was 2.3 km.

We propose that the location of the Lisan diapir, a large diapir within the Dead Sea pull-apart basin, in a sunken block of the basin can be explained by a model of diapiric formation during extension (Vendeville & Jackson, 1992a). According to this model, a diapir develops where the overburden was thinned relative to the surrounding area, provided the overburden is not too rigid and provided the viscosity of the salt is not too great to resist the rise. These conditions are met in the Dead Sea, where localized extension of the overburden is observed.

The Dead Sea basin was formed during the Miocene along the Dead Sea transform. Uncompacted sediment accumulation during the Miocene reached a thickness of about 1700 m in the study area. This was followed by the deposition of about 2.3 km thick evaporitic layer during the Pliocene. Rapid subsidence started however during the Pleistocene as attested by the accumulation of almost 4 km of Pleistocene sediments. We suggest that diapiric rise started in the early-to-middle Pleistocene during time of rapid N–S extension and subsidence of the central Dead Sea basin. Buried faults (Figs. 6 and 10) may be residual faults from this extension. Secondary E–W extension was promoted by the rapid subsidence because monoclinal draping of the cover over the large vertical step would create local stretching. The Lisan diapir initially grew much faster and wider than the Sedom diapir because rates of extension were much greater N–S along the long axis of the Dead Sea pull-apart basin than E–W across the basin. The overburden at the time of diapiric initiation is estimated at about 1 km thick. Rim synclines in the upper 1/3 of the overburden section indicate rapid withdrawal of salt from the central part of the basin during the middle to upper Pleistocene as the diapirs finally pierced the overburden.

The Amazyahu Fault is still rotating today indicating some N–S extension. Along it curved strike to the north, the Sedom diapir is rising vigorously. Diapiric rise would be promoted by the resultant local E–W compression,

squeezing the diapir laterally. In contrast, the N–S extension would retard the upward rise of the Lisan diapir, because salt will be used in lateral widening. The recent growth of the Lisan diapir is more complex with periods of growth punctuated by a longer period of stability. In general, however, the rate of extension and subsidence in this segment of the Dead Sea has probably slowed down relative to the earlier period, because we do not observe the fall or collapse of the diapir.

The study also provided additional details regarding the structure of this classical pull-apart basin. A previously suggested diagonal fault within the sediment overburden, the Boqeq Fault, is interpreted with the new data not to be a fault, but instead the edge of the diapir. Seismic data and gravity models indicate that the maximum basin depth, located under the Lisan peninsula, is ~8.5 km, about 1.5 km shallower than previously suggested. A narrow intermediate-depth block was discovered to extend along part of the eastern boundary of the basin and probably reflects block collapse into the deepest part of the basin.

Acknowledgements

A. Al-Zoubi's tenure at the Woods Hole Oceanographic Institution was funded by the Fulbright Exchange Program of the US Government. Special thanks to Jordan's Minister of Energy and Mineral Resources and the General Director of the Natural Resources Authority (NRA) for their permissions to carry this study outside Jordan. A. Al-Zoubi would like to thank the USGS/Woods Hole Field Center for opening their data archive for this study and for using their facilities, and the Woods Hole Oceanographic Institution/Department of Geology and Geophysics for their hospitality. The support of Mr Alan McNamara, head of the Fulbright office in Jordan and his staff is greatly appreciated. The General Director of Arab Potash Company has graciously opened some of his company's data archives for this study. Reviews by Bill Dillon, Dave Twichell, J. Christopher Harrison, and particularly, Martin P.A. Jackson, greatly improved the manuscript. Jeff Zwinakis drafted the figures.

References

Abu-Ajamieh, M. (1967). *Geophysical survey in the southern Jordan, Natural Resources Authority, Interior Report*, 41 pp.

Al-Khalidi, K., Abu Ayyash, K., Al-Nabulsi, S., & Sabha, M. (1997). *Petroleum exploration opportunities in Jordan*, Natural Resources Authority Press, 63 pp.

Alsop, G. I. (1996). Physical modelling of fold and fracture geometries associated with salt diapirism. In G. I. Alsop, D. J. Blundell & I. Davison. *Salt tectonics. Geological Society Special Publications*, 227–241.

Al-Zoubi, A. (2000). *Ground magnetic investigation of the Lisan Peninsula, Dead Sea*, *Interior Report of NRA*, Amman, Jordan.

Al-Zoubi, A., Shulman, H., & Ben-Avraham, Z. (2001). Seismic reflection profiles across the southern Dead Sea basin. *Tectonophysics*, in press.

Barton, D. C. (1933). Mechanics of formation of salt domes with special reference to Gulf Coast salt domes of Texas and Louisiana. *AAPG Bulletin*, *17*, 1025–1083.

Ben-Avraham, Z. (1997). Geophysical framework of the Dead Sea: Structure and tectonics. In T. M. Niemi, Z. Ben-Avraham & J. R. Gat, *The Dead Sea: the lake and its setting* (pp. 22–35). Oxford: Oxford University Press.

Ben-Avraham, Z., ten Brink, U. S., & Charrach, Y. (1990). Transverse faults at the northern end of the southern basin of the Dead Sea graben. *Tectonophysics*, *180*, 40–51.

Bender, F. (1974). *Geology of Jordan*, Berlin: Gebrueder Borntraegers, p. 196.

ten Brink, U. S., & Ben-Avraham, Z. (1989). The anatomy of a pull-apart basin: Seismic reflection observations of the Dead Sea basin. *Tectonics*, *8*, 333–350.

ten Brink, U. S., Ben-Avraham, Z., Bell, R. E., Hassouneh, M., Coleman, D. F., Andreasen, G., Tibor, G., & Coakley, B. (1993). Structure of the Dead Sea pull-apart basin from gravity analyses. *Journal of Geophysical Research*, *98*, 21,877–21,894.

ten Brink, U., Rybakov, M., Al-Zoubi, A., Hassouneh, M., Batayneh, A., Frieslander, U., Goldschmidt, V., Daoud, M., & Rotstein, Y. (1998). *Bouguer gravity anomaly map of the Dead Sea transform plate boundary in Israel and Jordan, scale 1:250,000*, *USGS open-file report*, pp. 98–516.

ten Brink, U., Rybakov, M., Al-Zoubi, A., Hassouneh, M., Batayneh, A., Frieslander, U., Goldschmidt, V., Daoud, M., Rotstein, Y., & Hall, J. K. (1999). The anatomy of the Dead Sea plate boundary: does it reflect continuous changes in plate motion? *Geology*, *27*, 887–980.

Csato, I., Kendall, C., Nairm, A., & Baum, G. (1997). Sequence stratigraphic interpretation in the southern Dead Sea basin, Israel. *Geological Society of America*, *109*, 1485–1501.

Folkman, Y. (1976). *Magnetic and gravity investigation of the crustal structure in Israel*. PhD thesis, Tel Aviv University, 203 pp.

Folkman, Y. (1981). Structural features in the Dead Sea–Jordan rift zone, interpreted from a combined magnetic-gravity study. *Tectonophysics*, *80*, 135–146.

Frieslander, U., & Ben-Avraham, Z. (1989). Magnetic field over the Dead Sea and vicinity. *Marine and Petroleum Geology*, *6* (2), 148–160.

Frumkin, A. (1996). Uplift rate relative to base-levels of a salt diapir (Dead Sea basin, Israel) as indicated by cave levels. In G. I. Alsop, D. J. Blundell & I. Davison. *Salt tectonics. Geological Society Special Publications*, 41–47.

Gardosh, M., Kashai, E., Salhov, S., Shulman, H., & Tannenbaum, E. (1997). Hydrocarbon exploration in the southern Dead Sea basin. In T. M. Niemi, Z. Ben-Avraham & J. R. Gat, *The Dead Sea: the lake and its setting* (pp. 57–72). Oxford: Oxford University Press.

Garfunkel, Z. (1997). The history and formation of the Dead Sea basin. In T. M. Niemi, Z. Ben-Avraham & J. R. Gat, *The Dead Sea: the lake and its setting* (pp. 36–56). Oxford: Oxford University Press.

Hall, J. K. (1993). The GSI digital terrain model (DTM) project completed. *Israel Geological Survey Current Research*, *8*, 47–60.

Hatcher, R. D., Zietz, I., Regan, R. D., & Abu-Ajamieh, M. (1981). Sinistral strike-slip motion on the Dead Sea rift: confirmation from new magnetic data. *Geology*, *9*, 458–462.

Horowitz, A. (1987). Palynological evidence for the age and rate of sedimentation along the Dead Sea Rift, and structural implications. *Tectonophysics*, *141*, 107–115.

Jackson, M. P. A., Roberts, D. G., & Snelson, S. (1995). *Salt tectonics a global perspective*, *AAPG Memoir, vol. 65*. Tulsa, OK: AAPG Press, 454 pp.

Kashai, E. L., & Croker, P. F. (1987). Structural geometry and evolution of the Dead Sea–Jordan Rift system as deduced from new subsurface data. *Tectonophysics*, *141*, 36–60.

Neev, D., & Hall, J. K. (1979). Geophysical investigations in the Dead Sea. *Sedimentary Geology*, *23*, 209–238.

Nettleton, L. L. (1934). Fluid mechanics of salt domes. *AAPG Bulletin*, *18*, 1175–1204.

Ram, E. (1989). *The magnetic field over the Dead Sea–Lisan area*. MS thesis, Tel Aviv University, 55 pp.

Rybakov, M., Goldshmidt, V., Fleischer, L., Rotstein, Y., & Goldberg, I. (1995a). Interpretation of gravity and magnetic data from Israel and adjacent areas. *Report no. R04/486/94*. Tel Aviv, Israel: The Institute of Petroleum Research and Geophysics.

Rybakov, M., Fleischer, L., & Goldshmidt, V. (1995b). A new look at the Hebron magnetic anomaly. *Israel Journal of Earth Sciences*, *44*, 41–49.

Rybakov, M., Goldshmidt, V., Rotstein, Y., Fleisher, L., & Goldberg, I. (1999). *Petrophysical constraints on gravity/magnetic interpretation in Israel*, *The Leading Edge*.

Seni, S. J., & Jackson, M. P. A. (1983). Evolution of salt structures, East Texas diapir province, part 2: patterns and rate of halokinesis. *AAPG Bulletin*, *67*, 1245–1274.

Stein, M., Starinsky, A., Agnon, A., Katz, A., Raab, M., Spiro, B., & Zak, I. (2000). The impact of brine–rock interaction during marine evaporite formation on the isotopic Sr record in the oceans: evidence from Nt. Sedom, Israel. *Geochimica et Cosmochimica Acta*, *64*, 2039–2053.

Trusheim, F. (1960). Mechanism of salt migration in northern Germany. *AAPG Bulletin*, *44*, 1519–1540.

Vendeville, B. C., & Jackson, M. P. A. (1992a). The rise of diapirs during thin-skinned extension. *Marine and Petroleum Geology*, *9*, 331–353.

Vendeville, B. C., & Jackson, M. P. A. (1992b). The fall of diapirs during thin-skinned extension. *Marine and Petroleum Geology*, *9*, 354–371.

Wawersik, W. R., & Zeuch, D. H. (1986). Modeling and mechanistic interpretation of creep of rock salt below 200 degrees C. *Tectonophysics*, *121*, 125–152.

Zak, I. (1967). *The geology of Mt Sedom*. PhD thesis, The Hebrew University, Jerusalem, 208 pp.

Zak, I., & Freund, R. (1981). Asymmetry and basin migration in the Dead Sea rift. *Tecotonophysics*, *80*, 27–38.